

Unraveling the Organization of the Internal Nuclear Matrix: RNA-Dependent Anchoring of NuMA to a Lamin Scaffold

Paola Barboro,* Cristina D'Arrigo,*† Alberto Diaspro,‡ Michele Mormino,† Ingles Alberti,* Silvio Parodi,*§ Eligio Patrone,† and Cecilia Balbi*¹

*Istituto Nazionale per la Ricerca sul Cancro, I-16132 Genova, Italy; †Istituto di Studi Chimico-Fisici di Macromolecole Sintetiche e Naturali, I-16149 Genova, Italy; ‡INFN, Dipartimento di Fisica, Università di Genova, I-16146 Genova, Italy; and §Dipartimento di Oncologia, Biologia e Genetica, Università di Genova, I-16132 Genova, Italy

Using quantitative immunoelectron microscopy we show here that when the nuclear matrix is isolated from rat hepatocytes in the presence of an inhibitor of RNase activity both lamins and the nuclear mitotic apparatus protein (NuMA) preferentially localize within the electron-dense domains of the internal nuclear matrix (INM). After RNA digestion NuMA undergoes a sharp depletion, while labeling by an antibody against lamins A and C within the electron-transparent regions increases, suggesting that a subset of lamin epitopes is masked by the interaction with RNA. We were able to explain this result by visualizing for the first time a thin web of lamin protofibrils which connects the electron-dense regions. Confirmation of these changes has been obtained by immunoblot analysis and confocal microscopy. As RNA digestion results both in the release of NuMA and in the collapse of the INM, we propose that a fraction of nuclear RNA brings about the association of NuMA islands with a lamin scaffold and that this interaction is required to maintain the latter in a state of high molecular dispersion. © 2002 Elsevier Science (USA)

Key Words: nuclear matrix; nuclear proteins; RNA; immunoelectron microscopy; confocal microscopy.

INTRODUCTION

The many vicissitudes in the development of isolation procedures capable of selectively extracting the constituents and preserving the structural features of the nuclear matrix are well known [1, 2]. Two early problems were the role of the intermolecular disulfide bonds in the stabilization of the intranuclear structures [3, 4] and the choice of the method to be employed for the digestion of chromatin and the mild extraction of the fragments [5–7] but, in retrospect, it was not

until resinless section electron microscopy was used to visualize the interior of the nuclear matrix (internal nuclear matrix (INM)) that major structural and biochemical features were revealed. The collapse which occurs after digestion of nuclear RNA suggested that the latter is an important structural component of the nucleus [8]. Moreover, the extraction of the RNA-containing (or complete) nuclear matrix with 2 M NaCl uncovered a network of 9- to 13-nm-thick core filaments, which retained 70% of nuclear RNA [9]. This substructure was impressively similar to the filamentous nucleoskeleton, composed of 11-nm-wide filaments with a 23-nm axial repeat, visualized in cells encapsulated in agarose by electron microscopy of resinless sections after electroeluting the chromatin fragments [7].

Recent advances in the unraveling of the protein composition of the INM by immunogold and immunofluorescence techniques have allowed the identification of the major structural components. Hozák *et al.* [10] have reported that in HeLa cells an anti-lamin A antibody recognizes nodes or knobs on the nucleoskeleton, while an antibody against lamin B labels foci on the nucleoskeleton only in a few nuclei. The presence of lamin A, but not of lamin B1, in the INM of human erythroleukemia cells has been recently described by Neri *et al.* [11]. In an embryonic mouse epidermal cell line, lamins A and B fused to the green fluorescence protein formed in interphase a veil of fluorescence within the nucleoplasm, suggesting that they can exist in a polymerized state all over the nucleus [12]. Evidence of the localization of nuclear mitotic apparatus protein (NuMA) isoforms in the core filaments of mammalian cells has been presented since 1994 [13]. Immunogold labeling with NuMA monoclonal antibodies of detergent-extracted interphase HeLa cells shows that the protein is scattered throughout the nucleoplasm; transient overexpression results in the formation of a regular nuclear lattice [14].

In this work we attempted to envisage an isolation method capable of avoiding the major pitfalls one

¹ To whom correspondence and reprint requests should be addressed at the Istituto Nazionale per la Ricerca sul Cancro, Largo Rosanna Benzi, 10; I-16132 Genova, Italy. Fax: (39) 010-5600217. E-mail: cecilia.balbi@istge.it.

meets in the course of the extraction of nuclear substructures. In the first place, we focused on the RNA-containing nuclear matrix [8]. Although the observation that the digestion of nuclear RNA removes the core filaments [9] has been revised [1], the induction of gross rearrangements of the INM remains an uncontroverted result [1, 7]. Second, experiments in which DNase I was used to digest chromatin showed that this enzyme exerts a destructive effect on the nucleoskeleton [7, 9]. Therefore we took advantage of the presence in rat liver nuclei of an endogenous nuclease which can be easily activated in the presence of Mg^{2+} and Ca^{2+} [15]; the digestion of isolated nuclei was followed by extraction in ammonium sulfate, which is known to efficiently solubilize the chromatin fragments [9]. No attempt was made to stabilize the INM by the sulfhydryl crosslinking reagent tetrathionate [4]. As a fact, in an early exploratory investigation using this crosslinking method, Kaufmann and Shaper [3] have reported that, after crosslinking, lamins could not be detected in the intranuclear network, in striking disagreement with the recent findings reported above. Instead, we isolated the nuclear matrix in the presence of 1 mM dithiothreitol (DTT) [16] to prevent the formation of disulfide bonds during the manipulation of the cells.

In this work the ultrastructural localization of lamins and NuMA was determined by a postembedding immunoelectron microscopy technique. The potential of the resinless approach in visualizing the major features of the nuclear architecture is beyond dispute; nevertheless, classical resin ultrathin section immunoelectron microscopy compares favorably with the resinless counterpart whenever quantitative work must be carried out, in that it allows one to carefully control the specificity of the labeling.

The results presented here show that lamins not only are the major components of the INM, but also form a thin fibrillar web, which is connected with a thick intranuclear network and extends throughout the electron-transparent regions of the nucleoplasm. As regards the involvement of RNA in the stabilization of the INM, we carefully monitored the ultrastructural and protein changes associated with RNA degradation. The digestion of the complete nuclear matrix with RNase induces an extensive depletion of NuMA, while the INM turns into large, chaotic aggregates, suggesting that nuclear RNA can play a dual structural role by bringing about the anchoring of NuMA islands to the lamin scaffold and by maintaining the latter in a state of high molecular dispersion.

MATERIALS AND METHODS

Antibodies. In the localization experiments by immunoelectron microscopy the following primary antibodies were used: the affinity-

purified goat polyclonal antibodies lamin A/C (N-18) and lamin B (C-20) (Santa Cruz Biotechnology, Inc.), which recognize peptides mapping at the amino terminus of human lamins A and C and at the carboxy terminus of human lamin B, respectively. The dilution of the antibodies was 1:15. For confocal microscopy the lamin A/C (N-18) antibody was used at a 1:20 dilution, while in Western blot analysis both the lamin A/C (N-18) and the lamin B (C-20) antibodies were employed (1:200 dilution). The monoclonal antibody against NuMA (Transduction Laboratories, Lexington, KY) was used in the immunoelectron microscopy, confocal microscopy, and Western blot experiments and was diluted 1:20, 1:10, and 1:150, respectively.

Rabbit anti-goat IgG (purchased from Sigma or from British Biocell International) was used for labeling lamins and goat anti-mouse IgG+IgM (British Biocell International) for NuMA. Either secondary antibody was conjugated with 10-nm gold particles. Normal rabbit serum was obtained from ICN Pharmaceuticals, Inc., and normal goat serum was purchased from British Biocell International.

Isolation of the nuclear matrix from rat hepatocytes. In order to minimize artifactual crosslinking of nuclear matrix proteins by disulfide bridges all the steps were carried out in the presence of 1 mM DTT [16]. Hepatocytes were prepared as reported in a previous paper [17] and nuclei isolated on a sucrose cushion exactly as described by Blobel and Potter [18] except that STM (250 mM sucrose, 5 mM $MgSO_4$, and 50 mM Tris-HCl, pH 7.4) was used instead of TKM (25 mM KCl, 5 mM $MgCl_2$, and 50 mM Tris-HCl, pH 7.5) containing 0.25 M sucrose. The nuclear pellet was resuspended in digestion buffer and digestion by the Ca^{2+}/Mg^{2+} -dependent endogenous nuclease allowed to proceed for 18 h [15]; chromatin fragments were extracted by adding $(NH_4)_2SO_4$ to a final concentration of 0.25 M [9]. The nuclear matrix retained ~2% of nuclear DNA. In some preparations the nuclei were digested in the presence of 2 mM vanadyl ribonucleoside complex (VRC) (GIBCO BRL) to prevent the activation of endogenous RNase. The pellet obtained after chromatin extraction was resuspended in 10 ml of digestion buffer containing 25 $\mu g/ml$ protease-free RNase A (Calbiochem) and digested for 10 min at 25°C; when the matrix was prepared in the presence of VRC the pellet was repeatedly washed with 75 mM NaCl, 24 mM Na_2EDTA to dissociate the inhibitor.

Electron microscopy and immunoelectron microscopy. Nuclear matrix pellets were washed three times in a solution containing 100 mM NaCl, 10 mM Tris-HCl (pH 7.5), 1 mM Na_2EDTA , 1 mM EGTA, fixed in 2.5% glutaraldehyde, and postfixed in OsO_4 ; embedding in Poly/Bed 812 resin (Polysciences, Inc., Warrington, PA) or Epon (Serva, Heidelberg, Germany), as well as sectioning and staining of the thin sections, was performed as already reported [17]. Ultrastructural localization of the major components of the INM was investigated by a postembedding immunogold labeling technique which exploits the capability of strong oxidizing agents such as sodium metaperiodate to reverse the masking effect that osmium tetroxide exerts on the antigenic sites [19, 20]. We have found that a brief etching of the sections with an alcoholic solution of NaOH [19, 21] followed by exposure to sodium metaperiodate greatly enhances the intensity of labeling and results in a highly specific and reproducible distribution of the gold particles, as judged from the values of the density of labeling ρ (number of gold particles/ μm^2) of defined nuclear substructures; furthermore, fine structural details appear to be fairly well preserved. Thin sections were mounted on nickel grids and etched with a 3% alcoholic solution of NaOH for 30 s, followed by successive 1-min treatments with 100, 95, 70, and 50% ethanol. All the incubations described below were carried out in a moist chamber. After a brief washing in distilled water the sections were incubated for 45 min on a saturated aqueous solution of sodium metaperiodate, rinsed in distilled water, and washed for 10 min with 2 drops of TBS1 buffer (150 mM NaCl, 50 mM Tris-HCl, pH 7.6) supplemented with 0.1% BSA (TBS1B). The sections were incubated for 30 min with normal serum of the same species as the secondary antibody diluted

1:20 in TBS1 and allowed to react overnight at 4°C with the primary antibody diluted in TBS1B. After being washed with 10 drops of TBS1B followed by 10 drops of TBS2 (150 mM NaCl, 20 mM Tris-HCl, pH 8.2) supplemented with 0.1% BSA (TBS2B), the sections were incubated for 1 h with the appropriate gold-conjugated secondary antibody diluted 1:10 in TBS2B. The sections were then rinsed in TBS2B and in distilled water, stained with 5% uranyl acetate in 50% ethanol followed by 0.4% aqueous lead citrate, and examined in a Zeiss LEO 900 electron microscope operating at 80 kV. The specificity of the immunolabeling was routinely assessed by omitting the incubation with the primary antibody. No significant labeling was detected, the labeling density ρ being on the order of 0.1 gold particle/ μm^2 . The specificity of the primary antibodies was tested prior to immunoelectron microscopy by Western blot analysis using complete nuclear matrix proteins; as an additional control for polyclonal lamin antibodies the latter were replaced with goat serum at the same concentration. We noticed that the major factor affecting the specificity of labeling was the aging of the antibodies stored at 4°C. As a rule, an appreciable increase in the intensity of labeling was observed after a 6- to 8-month storage, synchronous with the appearance of gold particles inside regions of pure resin far away from the specimen; lots of antibodies yielding values of ρ higher than ~ 1 particle/ μm^2 of resin were systematically discarded.

In some experiments both ultrastructural characterization and immunogold labeling were carried out on thin sections of embedded nuclei after *in situ* extraction of chromatin and RNA, following the same procedure used to isolate the nuclear matrix. After etching and exposure to metaperiodate, chromatin was digested directly on the grid with 50 μl of 2500 U/ml *EcoRI* and 500 U/ml *HaeIII* [22] in 130 mM KCl, 1 mM MgCl_2 , 1 mM DTT, 11 mM Na_2HPO_4 , pH 7.4, for 40 min at 25°C. After extraction of the chromatin with several drops of 0.25 M $(\text{NH}_4)_2\text{SO}_4$, the section was washed with 3 drops of distilled water; subsequent digestion with RNase A and immunogold labeling were carried out as described above. To visualize the thin lamin web the specimens were rotary shadowed with tungsten at an angle of 16° in an Edwards 306 vacuum coater equipped with a twin hearth electron beam source.

Quantitative analysis of the immunogold labeling distribution. To determine ρ_D and ρ_L , the densities of labeling within dense and loose domains of the INM, the distribution of the gold particles was analyzed with a Kontron Elektronik System Vidas apparatus version 2.1 using a program written by ourselves. Regions of 1 μm^2 of the nuclear section were directly acquired from the negatives of the electron micrographs. After correction for shading and low-frequency background, the enhanced image was thresholded to obtain the binary image of the total gold particles (GT). A segmented image (GD) was then generated by thresholding the enhanced image to obtain the dense domains in white against a dark background; the threshold gray levels were 0 and 175 and were kept constant in all of the measurements. A binary image of the gold particles within the dense domains was obtained by masking GT with GD; the area as well as the number of gold particles was measured automatically. The same parameters were calculated for the loose domains by the difference between GT and the image of the particles within the dense domains. From 30 to 50 randomly selected regions were analyzed per NM preparation. The Kolmogorof-Smirnov test was used to verify the normal distribution of the data; the statistical significance of the changes in the values of ρ_D and ρ_L induced by RNA digestion was evaluated by Student's *t* test.

Immunofluorescent staining and confocal microscopy. Nuclear matrix samples for confocal microscopy were prepared following the procedure of Neri *et al.* [11] with minor modifications. Briefly, nuclear matrices were resuspended in phosphate-buffered saline (PBS) containing 2% sucrose, sedimented at 150g for 5 min, and then plated onto 0.1% poly-L-lysine (Sigma)-coated glass slides; this and the subsequent steps were carried out at room temperature. The matrices were incubated for 30 min in order to enhance adhesion and

fixed for 30 min in freshly prepared 3.7% paraformaldehyde in PBS-sucrose. After a brief wash in PBS, the samples were incubated for 15 min in PBS containing 2% BSA to block nonspecific binding sites. Labeling of nuclear matrix proteins was carried out for 1 h in PBS containing 2% BSA with a mixture of the primary NuMA and lamin A/C antibodies diluted 1:10 and 1:20, respectively. The slides were washed with PBS for 5 min; this step was repeated two more times and the samples were allowed to react for 30 min with FITC-conjugated rabbit anti-mouse (DAKO) and Cy3-conjugated rabbit anti-goat (Sigma) antibodies diluted 1:10 and 1:40, respectively, in PBS containing 2% BSA.

Direct plating of isolated matrices onto glass slides for immunofluorescent staining might involve structural rearrangements. Recently, however, Neri *et al.* [11, 23] have convincingly shown that in nuclear matrices prepared from human erythroleukemia cells neither lamin A nor NuMA changed its intranuclear spatial distribution, independent of the extraction procedures and of the stabilization of the isolated nuclei by treatment with different metal ions or incubation at 37°C.

Parallel optical sections through the specimen were acquired by a Nikon PCM 2000 (Nikon Instruments, Florence, Italy) laser scanning microscope system; an argon-ion laser (488 nm) and a He-Ne laser (543 nm) source, enclosed in a common multilaser module, provided the excitation beams. Emitted fluorescence was revealed operating in dual-channel mode using a HQ590 (Chroma, Brattellboro, VT) and a HQ515 (Chroma). The sampling density at which the images were recorded was ~ 50 nm/pixel along the *x*, *y* axes, while the minimum sampling along the *z* axis was 200 nm; the Nyquist criterion was fulfilled both for lateral and for axial scanning. In order to perform intensity distribution analysis a subvolume of 16×16 pixels along with seven slices was selected. Frequency histograms for each specimen were obtained by summing the histograms slice by slice and normalizing with respect to the total count; histograms from 20 specimens per nuclear matrix preparation were finally averaged using the Origin version 4.00 program (Microcal Software, Inc.).

Quantitation of the major components of the nuclear matrix by Western blot analysis. The relative amounts of type A lamins, lamin B, and NuMA were determined following the quantitative Western blot method described in Alberti *et al.* [24]; peroxidase-conjugated anti-goat IgG (Santa Cruz Biotechnology, Inc.) and anti-mouse IgG+IgM (DAKO) were used to detect lamins and NuMA, respectively.

Miscellaneous. SDS-PAGE and high-resolution two-dimensional electrophoretic analysis of the nuclear matrix proteins were carried out as already described [24]. RNA and DNA were sequentially isolated from the same sample according to the Ambion Totally RNA isolation kit (Ambion, Inc., Austin, TX), dissolved in 0.1 N NaOH, and the concentration was determined from the absorbance at 260 nm assuming an extinction coefficient $E^{1\%} = 300$ for alkali-denatured DNA and $E^{1\%} = 250$ for RNA. Protein concentration was determined using the Bio-Rad Protein Assay (Bio-Rad, Munich, Germany) with BSA as a standard.

RESULTS AND DISCUSSION

Reexamining the Role of RNA in the Stabilization of the INM: Specific Morphological Rearrangements and Depletion of Heterogeneous Nuclear Ribonucleoproteins Are Associated with the Digestion of Nuclear RNA

Isolation procedures of the nuclear matrix which involve the degradation of RNA by exogenous RNase yield specimens showing an altered morphology compared with the RNA-containing counterpart [1]. One

explanation is that heterogeneous nuclear RNA in association with heterogeneous nuclear ribonucleoproteins (hnRNPs) represents the scaffolding structure of the INM. Another explanation is that heterogeneous nuclear RNA forms a substructure which is distinct from, but tightly interacts with, the scaffold, so affecting its physicochemical properties. If that is the case the observed effects would be determined by changes in the extent of aggregation of the latter, induced by the loss of the interaction with RNA.

The comparison between the morphologies of the INM isolated in the presence or absence of VRC (designated +VRC and -VRC, respectively) is reported in Fig. 1 and further details are shown in Figs. 2B, 2D, and 2F. The +VRC matrix (Fig. 1A) shows well-resolved spherical particles, from 15 to 35 nm in diameter, which are either closely associated or joined by short, irregular fibrillar segments (Figs. 1A and 2B); this characteristic morphological motif is referred to as the fibrogranular network [1]. Other regions of the nuclear interior seem empty and no substructure is visualized. In the absence of VRC the INM collapses, forming a thick, knobby network (Fig. 1B), and the globular elements are no longer visible (Fig. 2D). This process reaches its height with the formation of amorphous clumps; in some specimens the INM has the appearance of a tortuous, dense body, sharply delimited by extended empty regions (Fig. 1D). Essentially the same morphological alterations have been observed (Fig. 2F) when the nuclear matrix was isolated in the presence of VRC and subsequently digested with RNase A (+VRC, RNase matrix). In these experiments, however, clusters of granules survive digestion (arrows in Fig. 2F).

A relevant morphological detail is the presence, inside limited regions of the -VRC matrix, of poorly stained fibers (marked by arrowheads in Fig. 1C); an additional example, found in a -VRC matrix sample further digested with RNase A (-VRC, RNase matrix) is shown in the high-magnification electron micrograph reported in Fig. 1E. Several fibrillar stretches can be seen, connecting amorphous clumps of aggregated material. The fibers have cross dimensions of 12.2 ± 0.3 nm (mean \pm SE), which corresponds to the diameter of mature filaments of intermediate filament (IF) proteins [25].

The specific morphological features of the RNA-containing and RNA-depleted nuclear matrix can to some extent be observed in the inappropriate sample. For example, clumping can be clearly seen in Fig. 1B but is also present in Fig. 1A. On the basis of the scrutiny of several electron microscopic images we concluded that a limited morphological overlapping cannot be completely avoided, as it reflects the variability of the local concentrations of endogenous RNase and/or of VRC, which cannot be adequately controlled.

The hnRNPs remaining associated with both the +VRC and the -VRC matrix were detected by equilibrium two-dimensional gel electrophoresis; in some experiments samples of +VRC, RNase matrix were used to further evaluate the role of the integrity of nuclear RNA. Representative electrophoretic patterns are shown in Fig. 2. A few hnRNPs, designated hC1, hL, hU, and hK, can be easily identified on the basis of the values of the relative molecular weight and of the isoelectric point [26-28]. The electrophoretic pattern of the +VRC matrix clearly shows all of these components (Fig. 2A). The weight fractions of protein, DNA, and RNA, obtained by a reasonably accurate selective extraction method (limits of the SE \pm 5%) were found to be equal to 0.94, 0.02, and 0.04, respectively; these values represent the means of five determinations. The hnRNP spots are no longer visible in the -VRC matrix (Fig. 2C) excepting hnRNP-K, which is known to be a DNA binding protein [29], suggesting that these changes are a consequence of the digestion of nuclear RNA by endogenous RNase(s); this conclusion is supported by the composition data. The weight fractions of the major components were 0.96, 0.02, and 0.02, showing that \sim 50% of the RNA has been released with respect to the complete nuclear matrix. Finally, appreciable amounts of hnRNP-L are visible in the gel relative to the +VRC, RNase matrix (Fig. 2E), a result that is still correlated with the amount of residual RNA. Indeed, the nuclear matrix was found to be composed of 0.95 protein, 0.02 DNA, and 0.03 RNA, that is, to retain a high amount of RNA (\sim 75%), indicating that RNase A is unable to degrade all of the nuclear RNAs. Also the preservation of a few ultrastructural details (granules in Fig. 2F) is correlated with the higher content of residual RNA. The finding that RNase A does not efficiently digest all of the nuclear RNAs is by no means surprising. In a quantitative immunoelectron microscopy study of the affinity of several RNases for the RNAs localized in different cell compartments, Cheniclet and Bendayan [30] have shown that RNase A exhibits a higher affinity for cytoplasmic versus nucleoplasmic RNAs and, more importantly, fails to detect RNA without ambiguity in interchromatin granules, at variance with RNases T1 and T2. The pancreatic enzyme has, however, a preferential affinity toward the RNA molecules contained in perichromatin granules.

The extensive loss of the 15- to 35-nm granules can be directly related with the depletion of a subset of hnRNPs induced by RNA degradation. As a fact, the particles correspond in size to the hnRNP particles previously characterized in several laboratories. Thus, our experiments can be compared with confidence with previous observations [8] on the effect of RNA digestion both on the protein composition and on the morphology of the INM.

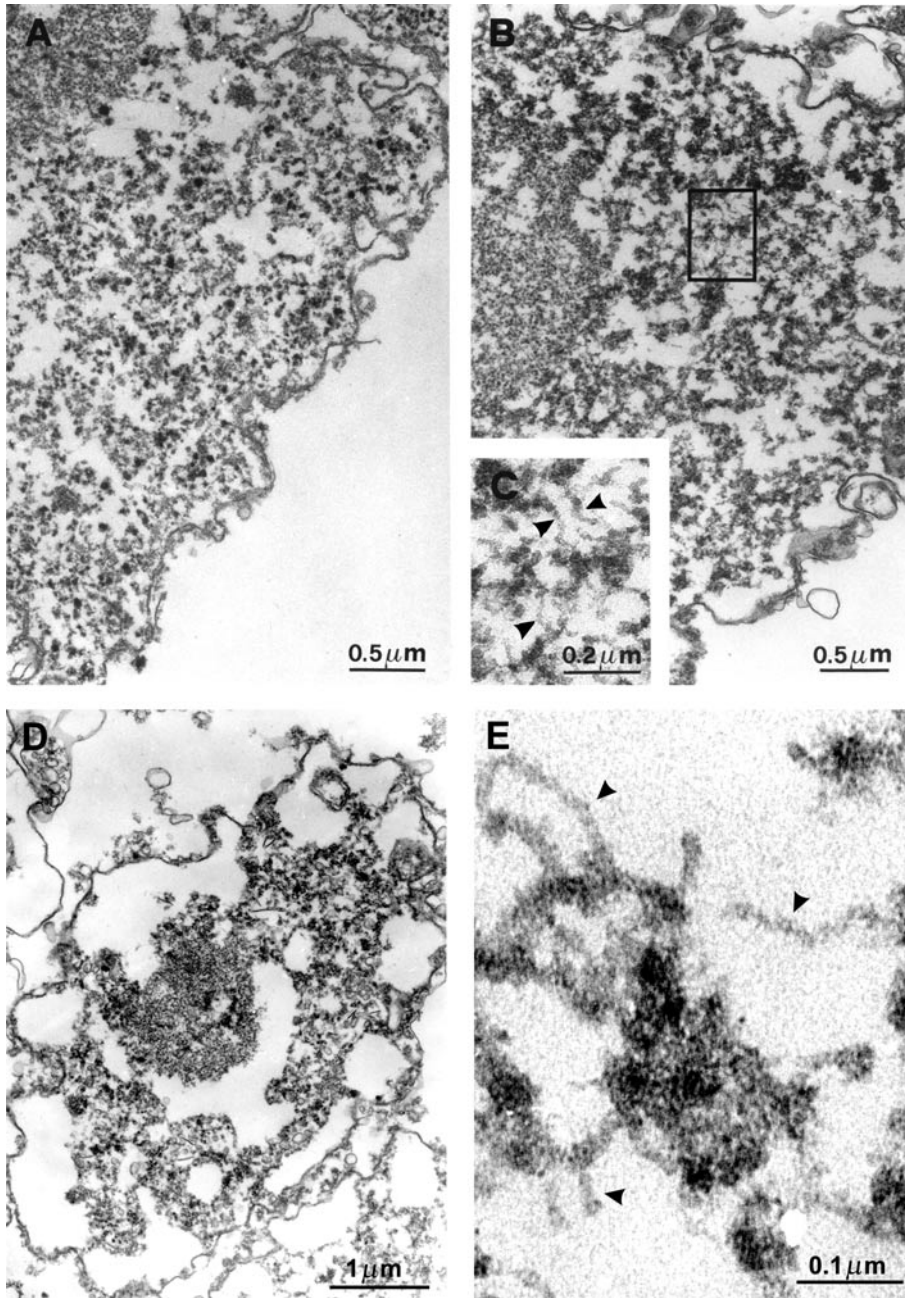


FIG. 1. Morphological changes of the INM induced by RNA digestion. Representative regions of +VRC (A) and -VRC (B, D) matrix samples; the aggregation and subsequent collapse of the INM are apparent in B and D, respectively. (C, E) Dark clumps of aggregated material connected by stretches of ~11-nm filaments (arrowheads), observed in samples of -VRC (C) and of -VRC, RNase matrix (E). C is a higher magnification of the area enclosed with lines in B. For the purpose of maintaining in the final print poorly stained details, the contrast was slightly decreased by scaling the gray levels in a Kontron Elektronik System Vidas apparatus.

RNA Digestion Releases NuMA, but Not Lamins, from the INM

As it has been recently suggested that both lamins [10] and NuMA [13] are components of the INM, we have attempted first to ascertain whether changes in the content of these proteins bear a relation to the

RNA-dependent morphological rearrangements described above; quantitation has been carried out by monodimensional immunoblot [24]. In an additional series of experiments, samples of -VRC, RNase matrix were also analyzed. No appreciable change in the amount of residual RNA was, however, found after

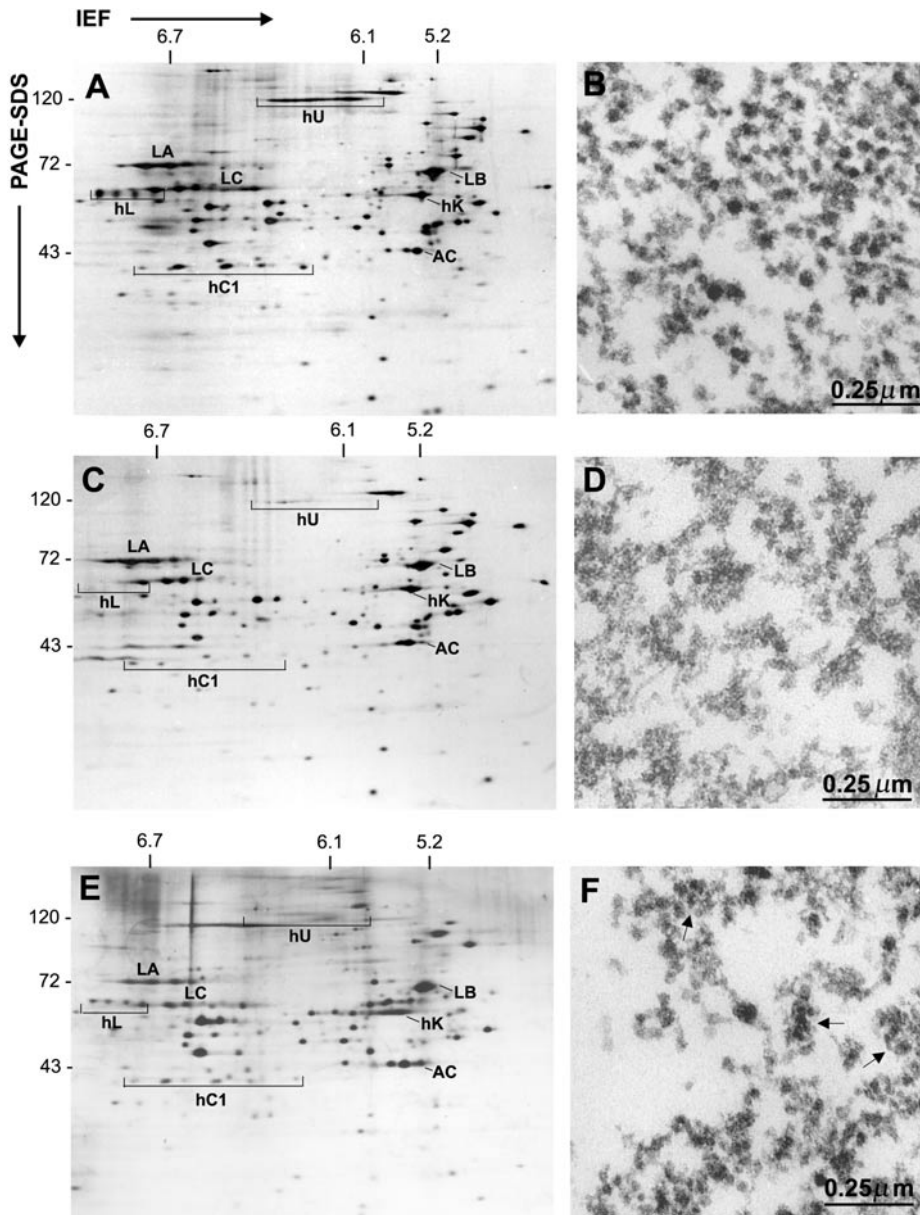


FIG. 2. Release of hnRNPs is correlated with the morphological alterations of the INM. (A, C, and E) Two-dimensional electrophoretic analyses of the proteins of the +VRC; -VRC; and +VRC, RNase matrix, respectively. The relative molecular weights of standard proteins in kilodaltons are reported on the left. (B, D, and F) Electron micrographs showing the morphologies of the same matrix preparations. The clusters of granules (B) are no longer observed (D) when all of the hnRNPs (except hnRNP-K) are extracted from the nuclear matrix (C). A few clusters, however (arrows in F), can be seen in the +VRC, RNase matrix, which retains appreciable amounts of hnRNP-L (E). L, lamins; AC, actin; h, hnRNP.

digestion, indicating that the endogenous RNase digests the RNase A-sensitive RNA fraction.

Representative immunoblot experiments are shown in Fig. 3A; the diagram in Fig. 3B illustrates the relative amounts of the proteins which remain associated with the matrix. In the case of lamins the values are not significantly affected by RNA degradation, while NuMA undergoes large changes. In fact, its relative amount decreases by $61 \pm 12\%$ (mean \pm SE) in the +VRC, RNase

and by 59 ± 9 and $72 \pm 13\%$ in -VRC and -VRC, RNase samples, respectively, compared with the +VRC matrix. No statistically significant differences among these values has been found using the Tukey *B* test.

This analysis shows that the fraction of NuMA which remains associated with the matrix critically depends on the integrity of RNA; indeed, digestion of the +VRC matrix releases $\sim 60\%$ of the protein while only 25% of the RNA is degraded. On the contrary, lamins are not lost

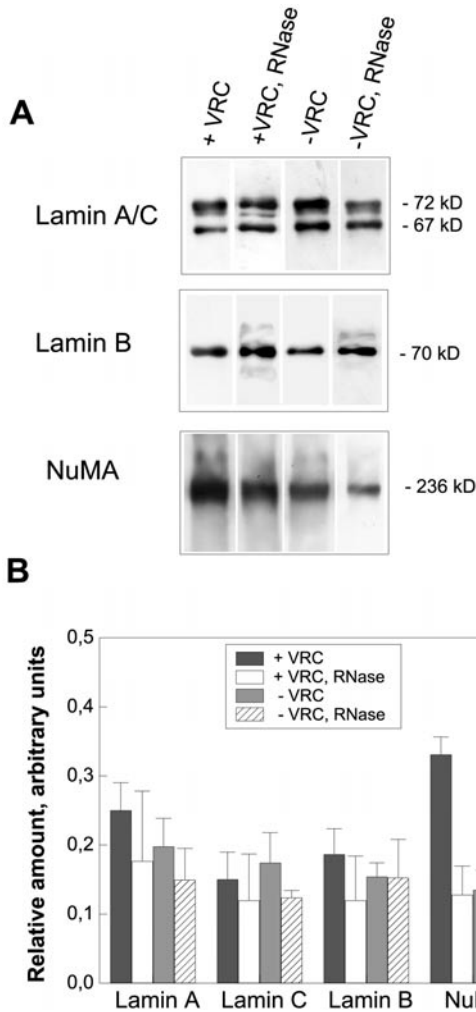


FIG. 3. RNA digestion releases NuMA but not from lamins from the RNA-containing INM. (A) Western blots using the lamin A/C, lamin B, and NuMA antibodies; the different matrix preparations are denoted as reported in Figs. 1 and 2. The relative molecular weights of the proteins are indicated on the right. The ordinates in (B) represent the mean \pm SE of the relative amounts of the lamins and NuMA in the different matrix preparations, determined by quantitative analysis of from four to eight samples. The relative amounts of lamins were found to be not significantly different using the Tukey *B* test ($P > 0.05$), while the decreases in the content of NuMA induced by RNA digestion in the +VRC, RNase; -VRC; and -VRC, RNase with respect to the +VRC matrix were found to be highly significant ($P = 0.008$, $P = 0.003$, $P = 0.002$, respectively).

in the course of RNA digestion and might therefore represent the building blocks of a permanent scaffolding structure.

The Epitopes of Lamins and NuMA Localize in the Electron-Dense Regions of the INM and Undergo Large and Definite Changes in the Distribution after RNA Digestion

In this section the +VRC matrix is compared with the RNA-depleted material isolated in the absence of

the inhibitor and digested with RNase A (-VRC, RNase). Although further digestion with the exogenous enzyme neither releases appreciable amounts of RNA nor affects the gross morphology of the INM, we have included this step in view of the fact that several investigations on the organization of the INM were concerned in the characterization of the RNase A-digested matrix; therefore, the results discussed here can be compared with the greatest possible confidence with the data reported in a large literature.

Electron microscopy images, clearly showing the distribution of the gold particles (which locate anti-lamin A and C and anti-NuMA antibody binding sites) between electron-dense and -transparent regions of the INM, are presented in Fig. 4. When the matrix is isolated in the presence of the RNase inhibitor the epitopes of both lamins A and C and NuMA are clustered inside the more dense domains, while the loose regions are labeled more weakly (Figs. 4A and 4C). RNA digestion affects in a different way the distribution pattern of the epitopes of lamins compared with that of NuMA. In the case of lamins the removal of RNA induces the appearance of several gold particles inside the loose regions of the INM; the dense domains undergo the morphological rearrangements already described, but there is no significant change in the density of labeling (Fig. 4B). The epitopes of NuMA, on the contrary, undergo an appreciable depletion in the electron-dense regions (Fig. 4D). These results strongly suggest that the loss of nuclear RNA unmasks several buried epitopes of lamins, while it induces the detachment of NuMA from the scaffold. Quantitation of these changes has been carried out by a careful image analysis procedure; the results are reported in Table 1. The data confirm that the epitopes of lamins A and C are preferentially located within the dense regions, as judged from the value (8.8 ± 0.5) of ρ_D/ρ_L , the ratio of the density of labeling in the dense to that in the loose regions; ρ_L undergoes a significant ($P < 10^{-4}$) increase from 87 ± 15 to 175 ± 8 as a consequence of RNA digestion, causing the ratio to drop to 4.7 ± 0.2 . The epitopes of NuMA are strongly localized in the dense regions and very few gold particles are found outside ($\rho_D/\rho_L = 56.5 \pm 8.8$); RNA digestion induces a significant ($P < 10^{-4}$) decrease (from 226 ± 12 to 71 ± 6) in ρ_D . On the basis of the decrease in the total labeling density ρ_T we can estimate that 62% of the NuMA molecules are removed, a value which is in good agreement with that previously determined by quantitative immunoblot analysis (72%). The data reported in Table 1 show also the interesting fact that $A_D\%$ represents a fixed percentage (31.5 ± 1.3) of the total area of the nuclear section, irrespective of the procedure used to isolate the matrix. As NuMA is among the most abundant components of the INM, we wondered why its large depletion did not affect the fraction of dense

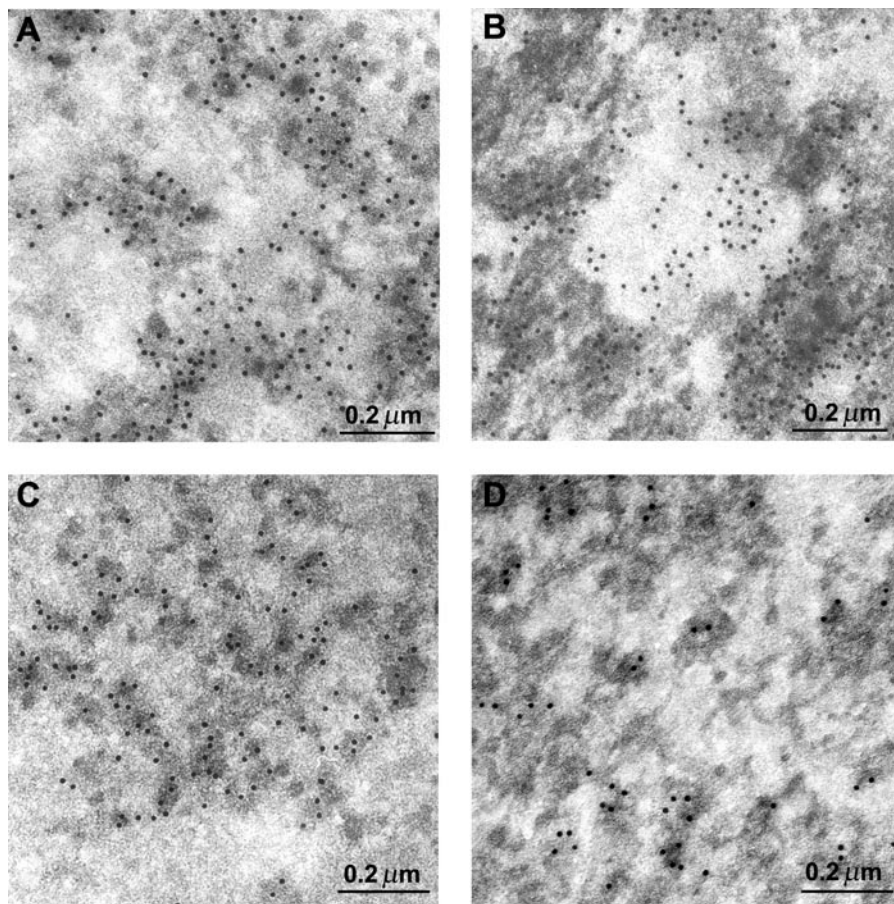


FIG. 4. The INM undergoes definite changes in the distribution of the epitopes of lamins A and C as well as of NuMA after RNA digestion. Samples of +VRC (A and C) and of -VRC, RNase matrix (B and D) were labeled using the lamin A/C (A and B) and the NuMA (C and D) antibody. Note that the gold particles are unevenly distributed between electron-dense and -transparent regions. The partial extraction of nuclear RNA unmasks several epitopes of lamins A and C inside the electron-transparent regions (B) and induces a strong depletion of the epitopes of NuMA in the dense domains of the INM (D).

domains. A basic stereological principle [31] states that the volume (or weight) fraction of a body (the dense domains) is equal to the surface fraction occupied by the body in a cross section ($A_D\%$). Utilizing the values 2×10^5 copies/nucleus for the abundance of NuMA [32] and 36.4×10^{-12} g for the total protein content of the rat liver nucleus [33] and considering that nuclear matrix proteins account for $\sim 12\%$ of the nuclear protein weight [5], we find that NuMA corresponds to $\sim 1.8\%$ of the matrix proteins. This value gives a contribution of 0.57 to $A_D\%$, which is well below the experimental uncertainty ($SE = 1.3$). We conclude that even if a 100% depletion of NuMA occurred, this change could hardly be detected by determinations of $A_D\%$. This consideration further supports the view that the gross morphological alterations observed after RNA digestion do not directly reflect the loss of material from the nucleoplasm, but represent extensive rearrangements of the INM induced by the suppression of the stabilizing effect exerted by nuclear RNA.

The distribution pattern of lamin B has not yet been characterized in detail. Preliminary data show that this protein also localizes in the electron-dense regions of the INM isolated in the presence of VRC ($\rho_D/\rho_L = 5.2$).

Nickerson [2], commenting on previous investigations on the composition of the core filaments by immunoelectron microscopy [10, 34], concluded that neither lamins nor NuMA is a good candidate for core proteins. On the contrary here we have shown, using a reliable and sensitive immunogold technique, that the INM contains all of the three lamins, in agreement with the conclusions drawn by Hozák *et al.* [10] from resinless and conventional immunoelectron microscopy observations, despite a somewhat low density of labeling. As regards NuMA, however, our results are in line with Nickerson's view. Both lamins and NuMA preferentially localize in the electron-dense domains of the INM, but extensive depletion of the latter (Fig. 4) occurs after RNA digestion. This coincidence could hardly be explained without the as-

TABLE 1

Distribution of the Gold Particles between Electron-Dense and -Transparent Regions of the INM for Complete and RNA-Depleted Nuclear Matrix.

Antibody against	Isolation conditions	Area (μm^2) ^a			Gold particles/ μm^{2b}			
		A_T	A_D	$A_D\%$ ^b	ρ_T	ρ_D	ρ_L	ρ_D/ρ_L
Lamins A and C	+VRC	40.1	12.7	33 ± 4	292 ± 8	767 ± 15	87 ± 15	8.8 ± 0.5
Lamins A and C	-VRC, RNase	43.1	13.4	34 ± 3	353 ± 13	814 ± 40	175 ± 8	4.7 ± 0.2
NuMA	+VRC	57.8	17.6	31 ± 1	68 ± 3	226 ± 12	4.3 ± 0.6	56.5 ± 8.8
NuMA	-VRC, RNase	59.4	19.9	28 ± 4	26 ± 2	71 ± 6	5.5 ± 0.7	12.9 ± 2.0

^a A_T is the total area analyzed and A_D the total area of the dense regions, determined using the image analysis method described under Materials and Methods.

^b The values are the means of from 30 to 50 determinations ± SE.

sumption that a large fraction of NuMA molecules, possibly in association with hnRNPs, forms a distinct substructure which is tightly bound to an underlying lamin scaffold as a consequence of its interaction with nuclear RNA; of course, at present, the involvement of additional RNA and/or lamin binding proteins cannot absolutely be ruled out. Furthermore, in the electron micrographs of RNA-depleted nuclear matrix morphological details can be seen which support the organization outlined above. The arrowheads in Figs. 1C and 1E indicate segments of poorly stained, 11-nm filaments associated with clumps of aggregated material, suggesting that the former consist of lamins and the latter of residual NuMA and hnRNPs; this motif recurs in both -VRC (Fig. 1C) and -VRC, RNase matrix samples (Fig. 1E). Interestingly, immunoelectron microscopy experiments by Nickerson, Krockmalnic, and Penman using three anti-NuMA antibodies (quoted in [2]) have show that the INM is labeled, but not the core filaments.

Confocal Microscopy Affords Direct Evidence of the Release of NuMA Induced by RNA Digestion

Two representative optical sections taken at the equatorial plane of isolated +VRC and -VRC, RNase matrices are shown in Fig. 5; red marks anti-lamin A/C epitopes, green anti-NuMA epitopes. The images show a somewhat broad red rim, which indicates that the matrix has undergone limited flattening. The central area, however, corresponding to the nucleoplasm is sharply defined, and no significant incidence of invaginations of the nuclear membrane has been detected by the scrutiny of sequential sections of several matrices from different preparations.

When the matrix is prepared in the presence of VRC, lamins show a very weak, diffuse fluorescence pattern confined to limited areas of the nucleoplasm (Fig. 5A), while NuMA staining is much more intense and organized in a spongy texture, resulting from sharp, clustered speckles standing out against a poorly stained

background (5B); by superimposing the images (5C) only a thin dotted rim surrounding the green area appears in yellow, as a consequence of the dominance of NuMA over lamin staining. The frequency distribution curve reported on the left of Fig. 5G confirms this result on a quantitative basis. The distribution of the relative fluorescence intensity of lamins is characterized by a modest skew and by a maximum which occurs at a low value of the intensity (~37), while NuMA shows a broad dependence of the frequency on the intensity with a maximum at ~140, indicating that NuMA clusters are extremely heterogeneous in size. The changes in the fluorescence pattern observed after digestion are in complete agreement with the results of Western blot analysis and of immunoelectron microscopy, in strong confirmation of the occurrence of depletion of NuMA and of the unmasking of lamin A and C epitopes. An increase in the staining of lamins is observed; the red fluorescence pattern consists of tiny dots scattered throughout the whole nucleoplasm (5D) while the frequency distribution curve (right in 5G) sharpens and undergoes a limited decrease (from ~37 to ~25) in the peak intensity, which suggests that the lamin substructure uncovered by RNA digestion has a very fine texture. On the contrary, there is a large loss of the staining signal of NuMA (5E), concomitant with the disappearance of the extended speckles present in Fig. 5B; this change corresponds to a fourfold decrease in the peak intensity (right in 5G). When the red and the green images are merged, the fraction of yellow area increases, so revealing that lamins and residual NuMA colocalize, in agreement with the immunoelectron microscopy experiments reported in the previous section, which show that both lamins and NuMA are mainly confined to the electron-dense regions of the INM. Also, dispersed red dots are present, likely corresponding to the electron-transparent areas in the electron micrographs, which are more intensely labeled by the lamin A/C antibody after RNA digestion

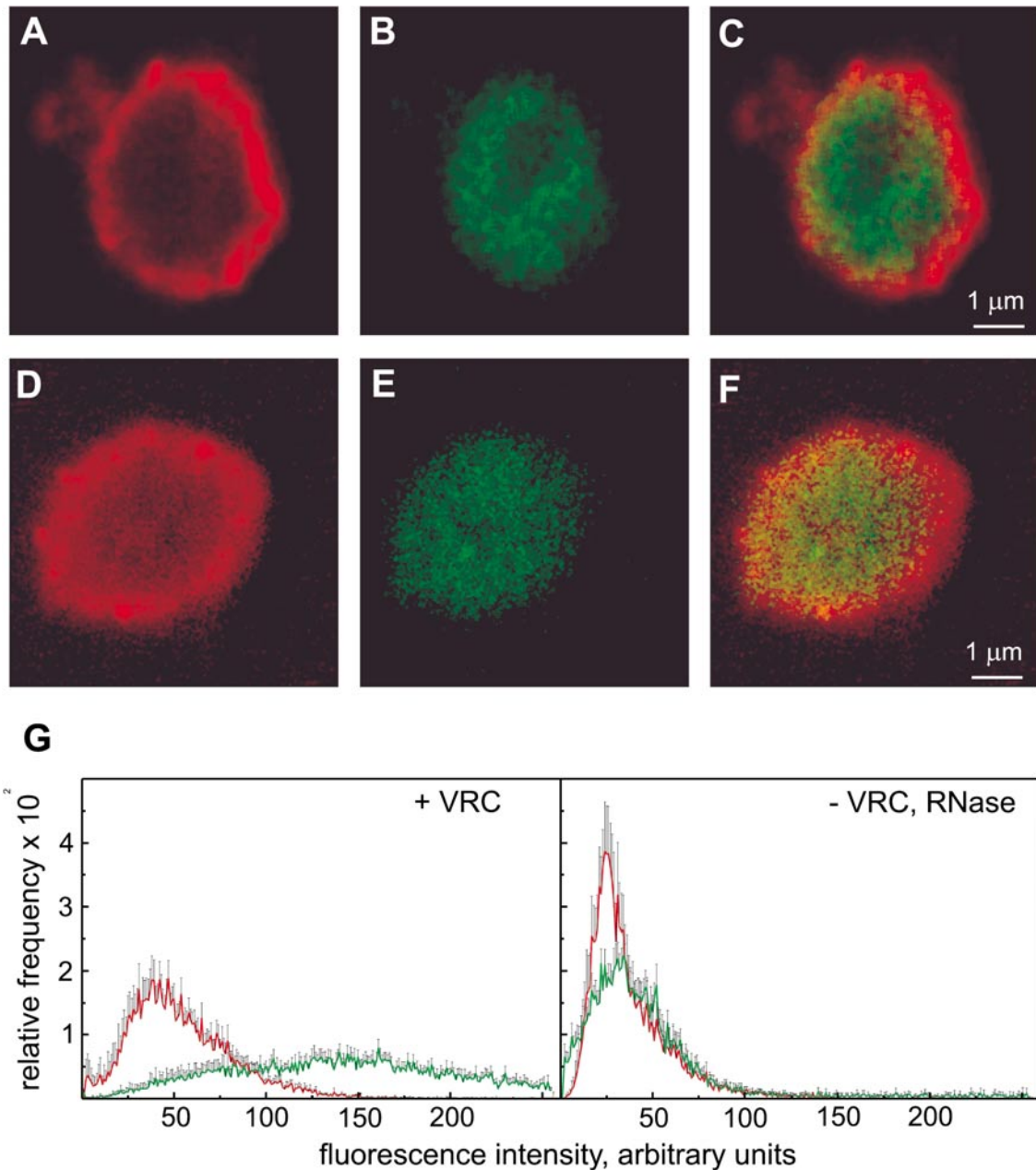


FIG. 5. Confocal microscopy directly shows that RNA brings about the anchoring of NuMA to an underlying lamin scaffold. (A–C) Complete (+VRC) and (D–F) RNA-depleted (–VRC, RNase) matrices were double labeled with the lamins A/C (red) and NuMA (green) antibodies. RNA digestion increases the red and strongly reduces the green signal (compare A with D and B with E). (C and F) Overlay images. The frequency distribution curves of the fluorescence intensity reported in (G) show this result on a quantitative basis. The strong decrease in the peak intensity of the green fluorescence induced by RNA digestion is consistent with the occurrence of a sharp reduction in the average size of the clusters of NuMA. The curves are the average of 20 determinations; the thin vertical lines indicate the SE.

and contain very few NuMA epitopes (Figs. 4B and 4D and Table 1).

In a previous paper Zeng *et al.* [13] have reported that NuMA remains tightly associated with the core filaments of HeLa cells after extensive extractions in solutions of 0.25–2.0 ionic strength, but undergoes dra-

matic rearrangements after RNA digestion. This observation is in line with the results of the thorough characterization reported here; these authors, however, did not comment on the occurrence of NuMA depletion. Because the cells were fixed in formaldehyde after digestion of RNA, in the absence of an intermediate

washing step, it is not surprising that no appreciable decrease in the immunofluorescence of NuMA has been detected in this study.

Lamins Form a Thin Fibrillar Web Which Connects the Dense Domains of the INM and Extends throughout the Electron-Transparent Regions

A puzzling outcome of the immunoelectron microscopy characterization using the lamin antibodies is the observation, inside the electron-transparent regions, of clusters of gold particles in the absence of any well-defined underlying structure (see for example Fig. 4B). This equivocal finding recurs in almost all of the electron microscopic images of RNA-depleted nuclear matrix as well as inside the limited "void" areas present in samples of complete nuclear matrix. Since careful controls to ascertain for the specificity of binding showed that our procedure was practically free from artifacts (see Materials and Methods), we concluded that the INM contains some fine substructure which cannot be adequately contrasted under standard embedding and/or staining conditions. Poly/Bed 812, a replacement of Epon, does not stain as readily as the original resin [35]; therefore, we embedded samples of -VRC matrix in a residual stock of Epon stored at -20°C . A representative electron micrograph is presented in Figs. 6A and 6B. Surprisingly, the "void" regions of the nucleoplasm appear to be filled with a very thin fibrillar web which reproduces, on a reduced scale, all of the morphological features of the network of core filaments [9] or of the nucleoskeleton [7]. The fibrils have transverse dimensions between 4.1 and 4.8 nm that correspond well to the diameter (4.5 nm) of the octameric protofibril, the major building block of the 10-nm IFs [25], and in certain regions split into two subfibrils (arrows in Fig. 6B) about 3 nm in transverse dimension, a value which is again comparable with the one of the IF tetrameric protofilament (2–3 nm).

As a rule we were unable to visualize the web in Poly/Bed 812-embedded samples by changing the staining conditions over a wide range. Since in the immunoelectron microscopy experiments etching strips the nuclear structures of the resin, the visibility of fine morphological details is expected to be enhanced in any sample simply by shadowing with heavy metals, after staining, etched specimens, provided that the effect of the alcoholic solution of NaOH is limited to the removal of a smooth resin layer. Matrix samples were etched and, after staining, shadowed with tungsten. The electron micrograph of a +VRC matrix sample reported in Fig. 6C clearly shows the thin fibrillar web connecting the dense regions. Although shadowing with tungsten results in an evaporated film of small grain size, the thin fibrils have unavoidably a dotted appearance which worsens somewhat the quality of the

image. Despite this minor limitation, however, shadowing provides the structural information we sought. After shadowing, the fine web was readily distinguishable in all of the Poly/Bed 812-embedded samples examined.

Finally we verified that the thin fibrils contain lamins. As mentioned above, the lamin A/C antibody recognizes several epitopes inside the void regions of both the complete and the RNA-depleted nuclear matrix embedded in Poly/Bed 812. Provided that the sample has been adequately contrasted, however, a thin web underlying the gold particles is clearly visualized; both the lamin A/C and the lamin B antibodies decorate the fine substructure, as documented by the high-resolution images reported in Figs. 7A, 7B, and 7C. The fibrils can be identified both in stained samples embedded in Epon (Fig. 7A), as expected, and in Poly/Bed 812 after staining and shadowing (Fig. 7B). A very infrequent result, namely, the visualization of the web in Poly/Bed 812-embedded samples in the absence of shadowing, is reported for comparison in Fig. 7C. The gold particles in most cases appear to be bound to the fibrils in a characteristic beads-on-a-string arrangement.

An additional feature of the two-dimensional distribution of the lamin epitopes is the existence of local order. The ordered array more frequently observed corresponds to rows of gold particles, which often extend for considerable distances (data not shown); the frequency distribution curve of the distances between adjacent particles is multimodal; the maxima occur at values that are multiples of ~ 25 nm, which corresponds to the axial repeat of lamin filaments and fibers assembled *in vitro* [25]. Measurements of the distances within a limited region of the fine web yield a comparable picture; for example, several nearby particles in Fig. 7C are at distances of 25.2 ± 0.2 and 47.5 ± 1.1 nm (means of eight determinations \pm SE, respectively). The quantitative analysis of local order can be used to put forward models for the assembly mode of lamins in the fine web and in the fibers, to be discussed in detail in a later paper.

In Situ Sequential Extraction of Poly/Bed 812-Embedded Nuclei Confirms the Key Structural Features of the Isolated INM

A problem that arises from the procedure used to isolate the nuclear matrix is whether the observed morphology corresponds to true architectural features or results from spurious rearrangements mainly occurring during the prolonged exposure to the digestion buffer. As the kinetics of the process is determined by the unrestrained motion of matrix subdomains, it can be frozen by anchoring the matrix to a stiff substrate. This condition is actually fulfilled, as shown previ-

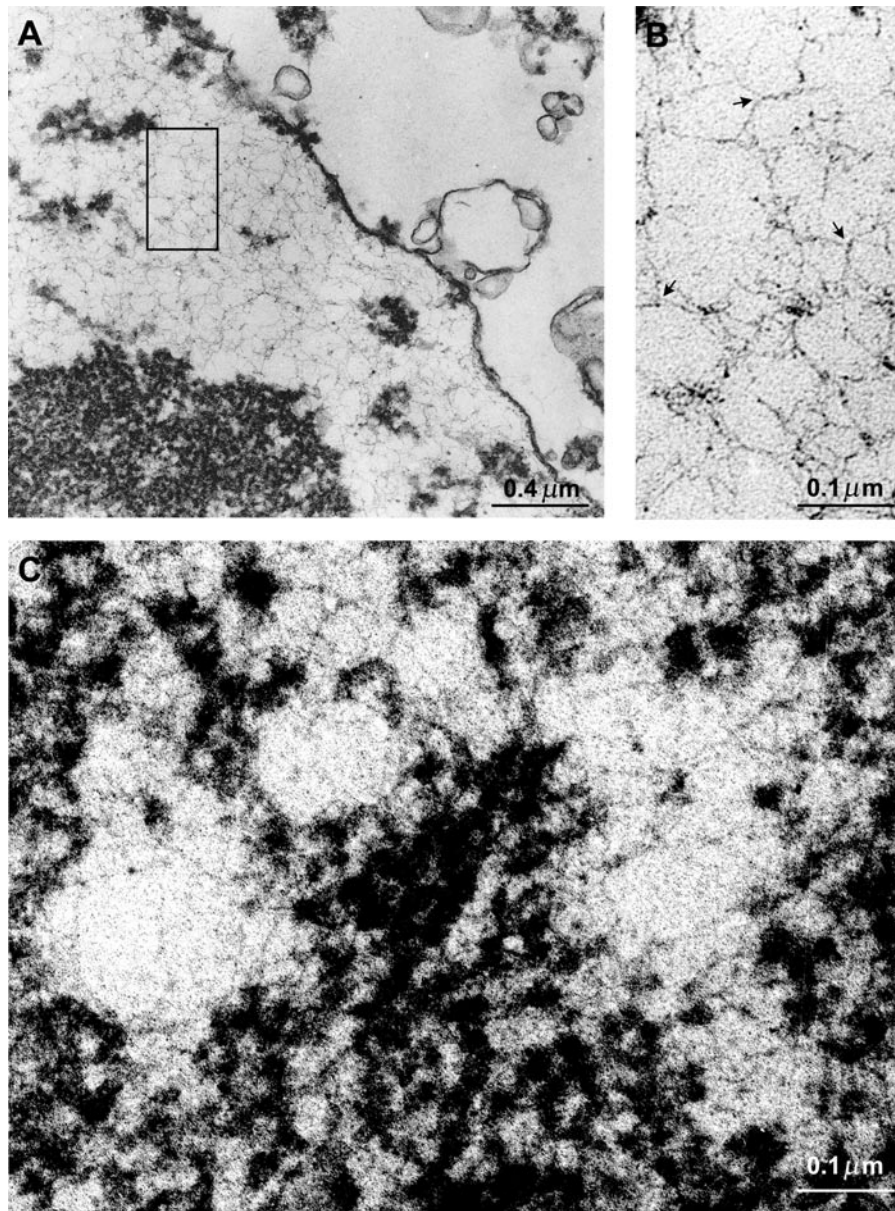


FIG. 6. Visualization of a thin fibrillar web inside the electron-transparent regions of the INM. (A) A web of thin (~ 4.5 and ~ 3 nm) fibrils visualized in an Epon-embedded sample of $-VRC$ matrix by staining with uranyl acetate and lead citrate. A high magnification of the area enclosed with a rectangle is shown in (B); the arrows indicate the splitting of a fibril into subfibrils. The same structure appears in Poly/Bed 812-embedded samples of $+VRC$ matrix submitted to etching and shadowed with tungsten after staining, in order to sharpen the imaging of the thin fibrillar web the contrast was enhanced by scaling the gray levels in a Kontron Elektronic System Vidas apparatus (C).

ously, when thin sections of resin-embedded matrix are etched with alcoholic NaOH; the resin is efficiently extracted, uncovering a layer of material which is still firmly bound to the bulk of residual resin. Therefore the occurrence of intranuclear aggregation can be circumvented by preparing the matrix *in situ* starting from resin-embedded nuclei. After etching, chromatin is removed by brief digestion with restriction enzymes and salt extraction. The results reported in the previous section show that this experiment is feasible. In

the first place, fine structural details are preserved after etching. Second, since etching followed by treatment with metaperiodate effectively restores the antigenic sites, it is quite reasonable to expect that this procedure causes also the recognition sites of the restriction enzymes to revert to the native conformation. Using this simple and direct approach we were able not only to verify that the key morphological motifs of the INM in nuclei extracted *in situ* are indistinguishable from those characterized in the isolated matrix, but

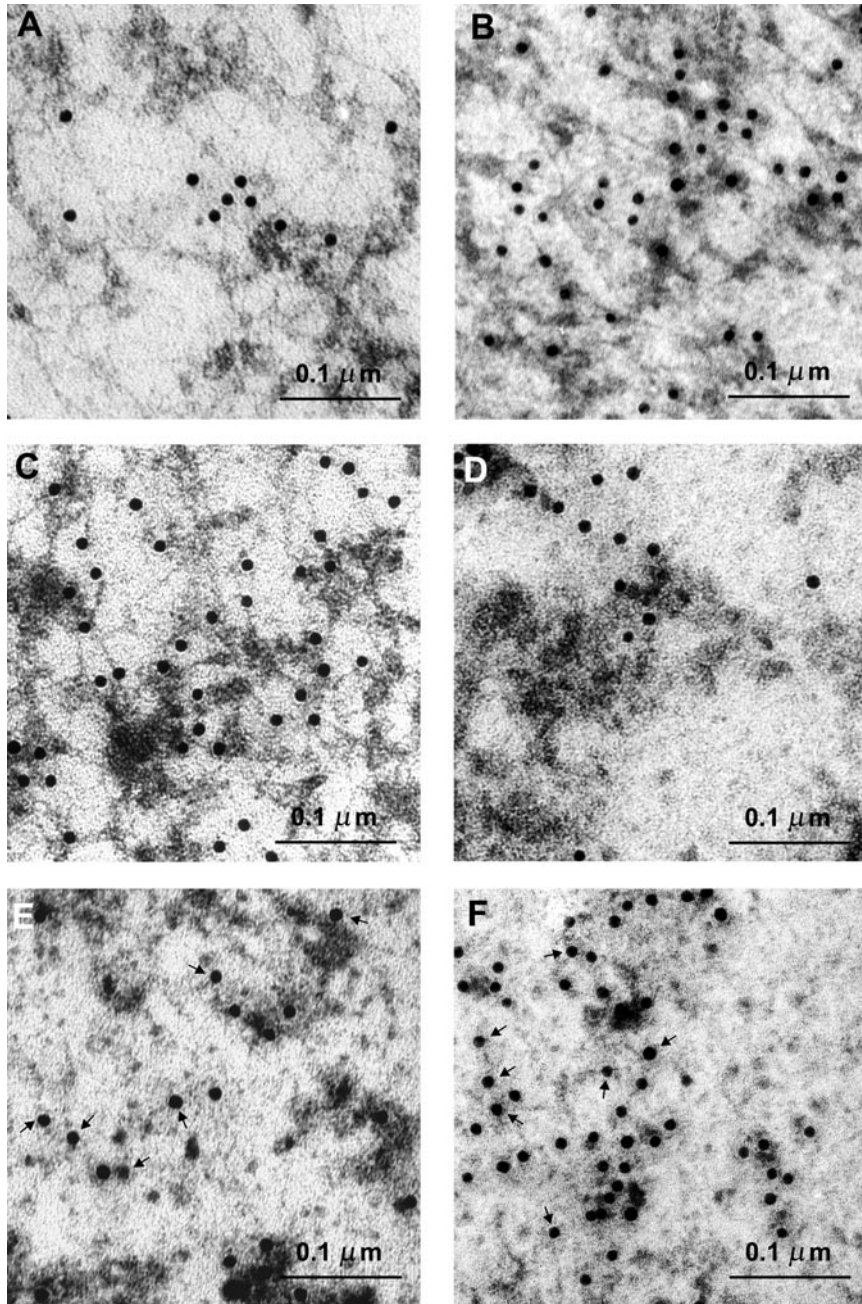


FIG. 7. Lamin antibodies recognize the thin fibrillar web both in the isolated matrix and in the resin-embedded nuclei after *in situ* extraction of chromatin and RNA. (A, B, and C) Isolated matrices. Highly specific recognition of the fibrils by the lamin A/C (A) and lamin B (B and C) antibodies is apparent in Epon-embedded -VRC matrix after staining (A), as well as in Poly/Bed 812-embedded +VRC matrix after staining followed by shadowing or, exceptionally, after staining alone (B and C, respectively). (D, E, and F) Nuclei extracted *in situ*. In undigested nuclei only a few gold particles are seen at the periphery of chromatin clumps (D) while after digestion with restriction enzymes the antibody decorates both the electron-dense regions and the thin fibrillar stretches (E); the number of the latter increases after RNA digestion (F). Poly/Bed 812-embedded nuclei; the specimens were shadowed after staining. (B, D, E, and F) Contrast enhancement as in Fig. 6C.

also to confirm the RNA-dependent sequential changes in the epitope distribution. In brief, the electron micrographs reported in Figs. 8A, 8B, and 8C show the relevant morphological changes resulting after extrac-

tion of the chromatin (Fig. 8B) and subsequent digestion of the RNA (8C); a progressive bleaching and sharpening of the intranuclear dense regions with respect to the undigested nucleus (8A) is apparent. Prior

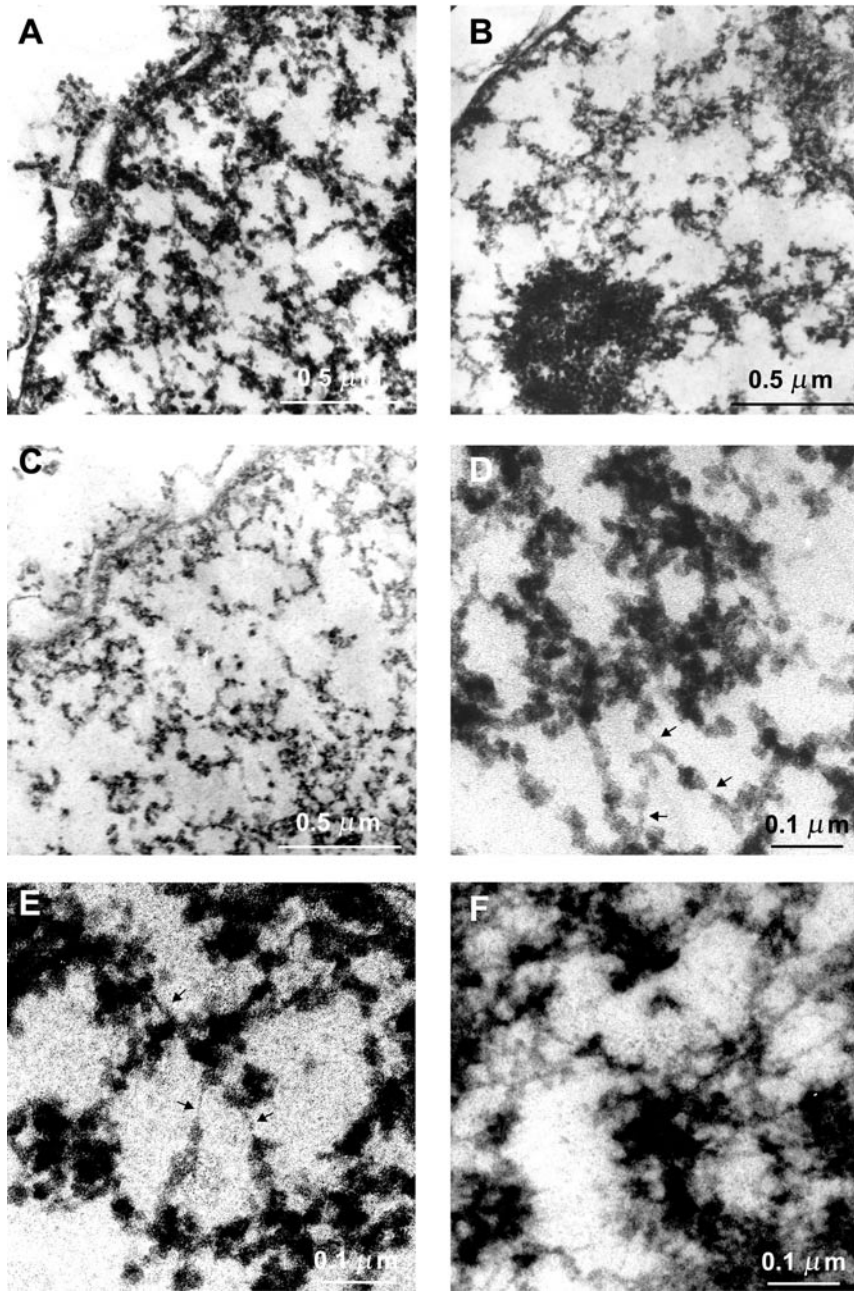


FIG. 8. Visualization of the architecture of the INM in resin-embedded nuclei by stepwise extraction of chromatin and RNA. (A, B, and C) Low-magnification images of Poly/Bed 812-embedded nuclei showing the overall changes in the morphology after chromatin extraction (B) and further digestion of RNA (C) with respect to undigested nuclei (A). Only short fibrillar segments are seen prior to digestion of DNA (arrows in D), while naked fibrils (arrows in E) and extended regions containing the fine web (F) come out after digestion of DNA and of both DNA and RNA, respectively. The samples were shadowed after staining. Contrast enhancement as in Fig. 6C.

to digestion of the chromatin only a few thin fibrillar stretches connecting poorly stained roundish bodies are observed (arrows in Fig. 8D); the lamin A/C antibody is excluded from and localized at the periphery of the dense chromatin domains (Fig. 7D). After extraction of the chromatin several thin filaments come out (arrows in Fig. 8E), while the antibody decorates both

the filaments and the dense regions (arrows in Fig. 7E), in agreement with the distribution observed inside the complete nuclear matrix. Digestion with RNase A greatly increases the proportion of naked filaments, resulting in the appearance of an extended web (Fig. 8F), while labeling inside the electron-transparent regions becomes more intense (Fig. 7F); gold particles

lining thin fibrils are marked by arrows. The sharpness of the images of the thin web is not as high as that characteristic of Epon-embedded matrices (Figs. 6A and 6B). In addition to the noise introduced by shadowing, undigested chromatin increases the dark background, while residual resin can form a veil that locally interrupts the path of the fibrils. Nevertheless, the micrographs presented in Figs. 7 and 8 directly support the contention that the lamin web is not an artifact involved in the isolation procedure.

Finally, experiments using the antibody against NuMA confirm that this protein is bound to a lamin scaffold and released after digestion of a fraction of nuclear RNA. In undigested nuclei the chromatin prevents the antibody from binding to the underlying structure (Fig. 9A). Extensive labeling of the dense regions occurs after extraction of the chromatin; large NuMA islands are frequently observed (Fig. 9B), together with a diffuse decoration mainly scattered all over the dense regions. After RNA digestion labeling undergoes an appreciable decrease concomitant with the disappearance of the large islands (Fig. 9C), in line with the outcomes of the quantitative analysis carried out by confocal microscopy.

Although the existence of a fine lamin web has been reported for the first time in this work, overall our results on the intranuclear distribution of lamins are not opposed to previous structural observations on the INM [7, 9]. This statement might be questioned, as we do not provide evidence of the existence of a network of 11-nm filaments. As already pointed out by Hozák *et al.* [10], however, it is difficult to visualize the nucleoskeleton in thin sections of resin-embedded samples; for this result to be attained the employment of 150- to 300-nm-thick resinless sections is required [7]. In this work the resin thickness is ~ 50 nm, which is much less than the average distance between branch points in the nucleoskeleton (see for example Fig. 4 in the paper quoted above). It is therefore not surprising that we were able to clearly visualize ~ 11 -nm-thick fibrillar stretches (Figs. 1C and 1E), while their assembly into a net could not be evidenced.

What the functional role of the web of thin fibrils might be remains an open question. This architectural feature might be essential for maintaining the INM in a state of high molecular dispersion for the control of the complex biochemical events occurring inside the nucleus. In putting forward this hypothesis, however, the instability over time of the fine web should be taken into account. Assembly experiments of lamins *in vitro* show that protofilaments and protofibers tend to associate into fibers or thick paracrystals [25] and this tendency toward aggregation actually accounts for the collapse of the INM after RNA digestion. Indeed, the visualization of extensive regions of fibrillar web in RNA-depleted matrices is a rather infrequent finding,

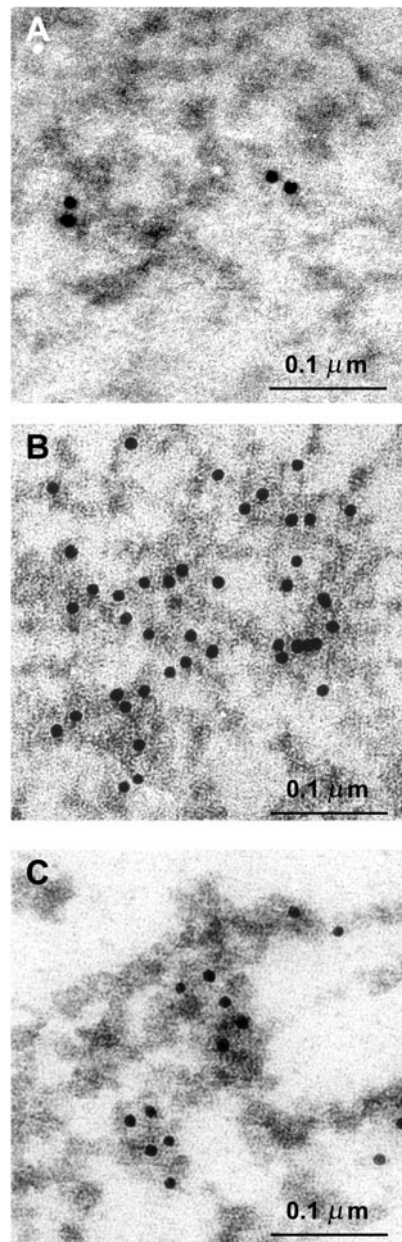


FIG. 9. In resin-embedded nuclei many of the epitopes of NuMA are unmasked by DNA digestion and undergo depletion after digestion with RNase A. (A) Undigested nuclei. Extended islands of NuMA appear after DNA digestion (B) but are no longer observed after digestion with RNase A. (C) Poly/Bed 812-embedded samples. The specimens were not shadowed in order to enhance the visibility of the gold particles against the dark background.

reflecting some delay in the onset of intranuclear rearrangements: also the preparation in which the specimen reported in Fig. 6A was detected consisted to a great extent of matrices showing a condensed morphology, similar to that apparent in Fig. 1B (data not shown).

These observations taken together further strengthen

the view that the interaction of the fibrillar web with RNA represents a critical factor in the structural stabilization of the INM. The molecular basis of this interaction remains to be discovered; as already noted, additional proteins or protein/RNA complexes could be involved. Alternatively, according to an attractively simple model, RNA might directly mediate the anchoring of NuMA to the lamin scaffold. If this hypothesis is correct, lamins and NuMA should show a high affinity of binding to RNA. To date, the above proteins have not been characterized as far as this relevant property is concerned. However, we wish to call attention to a careful competition study by Ludérus [36], which provides evidence of a significant competing effect of RNA from HeLa cells on the specific binding of matrix attachment region fragments to rat liver lamins.

This work was supported by the Italian Association for Cancer Research, the Ministero della Sanità, and the Ministero dell'Università e della Ricerca Scientifica e Tecnologica (MURST).

REFERENCES

- Nickerson, J. A., Blencowe, B. J., and Penman, S. (1995). The architectural organization of nuclear metabolism. *Int. Rev. Cytol.* **162A**, 67–123.
- Nickerson, J. A. (2001). Experimental observations of a nuclear matrix. *J. Cell Sci.* **114**, 463–474.
- Kaufmann, S. H., and Shaper, J. H. (1984). A subset of non-histone nuclear proteins reversibly stabilized by the sulfhydryl cross-linking reagent tetrathionate: Polypeptides of the internal nuclear matrix. *Exp. Cell Res.* **155**, 477–495.
- Stuurman, N., Meijne, A. M., van der Pol, A. J., de Jong, L., van Driel, R., and van Renswoude, J. (1990). The nuclear matrix from cells of different origin; Evidence for a common set of matrix proteins. *J. Biol. Chem.* **265**, 5460–5465.
- Berezney, R., and Coffey, D. S. (1974). Identification of a nuclear protein matrix. *Biochem. Biophys. Res. Commun.* **60**, 1410–1417.
- Mirkovitch, J., Mirault, M. E., and Laemmli, U. K. (1984). Organization of the higher-order chromatin loop: Specific DNA attachment sites on nuclear scaffold. *Cell* **39**, 223–232.
- Jackson, D. A., and Cook, P. R. (1988). Visualization of a filamentous nucleoskeleton with a 23 nm axial repeat. *EMBO J.* **7**, 3667–3677.
- Fey, E. G., Krochmalnic, G., and Penman, S. (1986). The non-chromatin substructures of the nucleus: The ribonucleoprotein (RNP)-containing and RNP-depleted matrices analyzed by sequential fractionation and resinless section electron microscopy. *J. Cell Biol.* **102**, 1654–1665.
- He, D. C., Nickerson, J. A., and Penman, S. (1990). Core filaments of the nuclear matrix. *J. Cell Biol.* **110**, 569–580.
- Hozák, P., Sasseville, A. M., Raymond, Y., and Cook, P. R. (1995). Lamin proteins form an internal nucleoskeleton as well as a peripheral lamina in human cells. *J. Cell Sci.* **108**, 635–644.
- Neri, L. M., Raymond, Y., Giordano, A., Capitani, S., and Martelli, A. M. (1999). Lamina A is part of the internal nucleoskeleton of human erythroleukemia cells. *J. Cell. Physiol.* **178**, 284–295.
- Moir, R. D., Yoon, M., Khuon, S., and Goldman, R. D. (2000). Nuclear lamins A and B1: Different pathways of assembly during nuclear envelope formation in living cells. *J. Cell Biol.* **151**, 1155–1168.
- Zeng, C., He, D., and Brinkley, B. R. (1994). Localization of NuMA protein isoforms in the nuclear matrix of mammalian cells. *Cell Motil. Cytoskeleton* **29**, 167–176.
- Gueth-Hallonet, C., Wang, J., Harborth, J., Weber, K., and Osborn, M. (1998). Induction of a regular nuclear lattice by overexpression of NuMA. *Exp. Cell Res.* **243**, 434–452.
- Balbi, C., Sanna, P., Barboro, P., Alberti, I., Barbesino, M., and Patrone, E. (1999). Chromatin condensation is confined to the loop and involves an all-or-none structural change. *Biophys. J.* **77**, 2725–2735.
- Gerace, L., Comeau, C., and Benson, M. (1984). Organization and modulation of nuclear lamina structure. *J. Cell Sci. Suppl.* **1**, 137–160.
- Barboro, P., Pasini, A., Parodi, S., Balbi, C., Cavazza, B., Allera, C., Lazzarini, G., and Patrone, E. (1993). Chromatin changes in cell transformation: Progressive unfolding of the higher-order structure during the evolution of rat hepatocyte nodules. A differential scanning calorimetry study. *Biophys. J.* **65**, 1690–1699.
- Blobel, G., and Potter, V. R. (1966). Nuclei from rat liver: Isolation method that combines purity with high yield. *Science* **154**, 1662–1665.
- Bendayan, M., and Zollinger, M. (1983). Ultrastructural localization of antigenic sites on osmium-fixed tissues applying the protein A-gold technique. *J. Histochem. Cytochem.* **31**, 101–109.
- Vardell, I. M., and Polak, J. M. (1987). EM immunolabelling. In "Electron Microscopy in Molecular Biology" (J. Somerville and U. Scheer, Eds.), pp. 179–200. IRL Press, Oxford/Washington, DC.
- Bergersen, L., Johannsson, E., Veruki, M. L., Nagelhus, E. A., Halestrap, A., Sejersted, O. M., and Ottersen, O. P. (1999). Cellular and subcellular expression of monocarboxylate transporters in the pigment epithelium and retina of the rat. *Neuroscience* **90**, 319–331.
- Hozák, P., Hassan, A. B., Jackson, D. J. A., and Cook, P. R. (1993). Visualization of replication factories attached to a nucleoskeleton. *Cell* **73**, 361–373.
- Neri, L. M., Bortul, R., Zwyer, M., Tabellini, G., Borgatti, P., Marchisio, M., Bareggi, R., Capitani, S., and Martelli, A. M. (1999). Influence of different metal ions on the ultrastructure, biochemical properties, and protein localization of the K562 cell nuclear matrix. *J. Cell. Biochem.* **73**, 342–354.
- Alberti, I., Barboro, P., Barbesino, M., Sanna, P., Pisciotto, L., Parodi, S., Nicolò, G., Boccardo, F., Galli, S., Patrone, E., and Balbi, C. (2000). Changes in the expression of cytokeratins and nuclear matrix proteins are correlated with the level of differentiation in human prostate cancer. *J. Cell. Biochem.* **79**, 471–485.
- Stuurman, N., Heins, S., and Aebi, U. (1998). Nuclear lamins: Their structure, assembly, and interactions. *J. Struct. Biol.* **122**, 42–66.
- Peters, K. E., and Commings, D. E. (1980). Two-dimensional gel electrophoresis of rat liver nuclear washes, nuclear matrix, and hnRNA proteins. *J. Cell Biol.* **86**, 135–155.
- Faura, M., Renau-Piqueras, J., Bachs, O., and Bosser, R. (1995). Differential distribution of heterogeneous nuclear ribonucleoproteins in rat tissues. *Biochem. Biophys. Res. Commun.* **217**, 554–560.

28. Mattern, K. A., Humbel, B. M., Muijsers, A. O., de Jong, L., and van Driel, R. (1996). hnRNP proteins and B23 are the major proteins of the internal nuclear matrix of HeLa S3 cells. *J. Cell. Biochem.* **62**, 275–289.
29. Tomonaga, T., and Levens, D. (1995). Heterogeneous nuclear ribonucleoprotein K is a DNA-binding transactivator. *J. Biol. Chem.* **270**, 4875–4881.
30. Cheniclet, C., and Bendayan, M. (1990). Comparative pyrimidine- and purine-specific RNase-gold labeling on pancreatic acinar cells and isolated hepatocytes. *J. Histochem. Cytochem.* **38**, 551–562.
31. Fullman, R. L. (1953). Measurement of particle size in opaque bodies. *Trans AIME* **197**, 447–452.
32. Compton, D. A., Szilak, I., and Cleveland, D. W. (1992). Primary structure of NuMA, an intranuclear protein that defines a novel pathway for segregation of proteins at mitosis. *J. Cell Biol.* **116**, 1395–1408.
33. Altman, P. L., and Katz, D. D., Eds. (1976). “Cell Biology,” pp.370–379. Federation of American Societies for Experimental Biology, Bethesda, MD.
34. He, D. C., Zeng, C., and Brinkley, B. R. (1995). Nuclear matrix proteins as structural and functional components of the mitotic apparatus. *Int. Rev. Cytol.* **162B**, 1–74.
35. Dykstra, M. J. (1993). “A Manual of Applied Techniques for Biological Electron Microscopy,” pp. 42. Plenum, New York/London.
36. Ludérus, M. E., den Blaauwen, J. L., de Smit, O. J., Compton, D. A., and van Driel, R. (1994). Binding of matrix attachment regions to lamin polymers involves single-stranded regions and the minor groove. *Mol. Cell. Biol.* **14**, 6297–6305.

Received March 14, 2002

Revised version received July 8, 2002

Published online August 19, 2002